MedChemComm

Accepted Manuscript

ROYAL SOCIETY OF CHEMISTRY

www.rsc.org/medchemcomm

Mechanism of forming trimer, self-assembling nano-particle and inhibiting tumor growth of small molecule CIPPCT

Fengxiang Du,[†] Xiaoyi Zhang,[†] Shan Li,[†] Yaonan Wang,[†] Meiqing Zheng,[†] Yuji Wang,[†] Shurui Zhao,[†] Jianhui Wu,[†] Lin Gui,[†] Ming Zhao,*[†, ‡] Shiqi Peng*[†]

[†]College of Pharmaceutical Sciences, Capital Medical University, Beijing 100069, P.R. China.

[‡]Department of Biomedical Science and Environmental Biology, Kaohsiung Medical University, Kaohsiung, Taiwan

*To whom correspondence should be addressed. **SP**: College of Pharmaceutical Sciences, Capital University of Medical Sciences, Beijing 100069, P.R. China. Tel: 86-10-8391-1528, Fax: 86-10-8391-1528, E-mail: sqpeng@bjmu.edu.cn; **MZ**: Tel.: +86-10-8280-2482, fax: +86-10-8280-2482, E-mail: mingzhao@bjmu.edu.cn

Abstract The mechanisms of small molecules forming nano-species and the effect of the nano-species of small molecules on their pharmacological actions remain to be elucidated. As one of our efforts here a uPA inhibitor, (5aS,12S,14aS)-5,14-dioxo-12-(2-tryptophanylthreo-nylbenzylester-N-yl-ethyl-1-yl)-1,2,3,5,5a,6,11,12,14,14a-decahydro-5H,14H-pyrolo[1,2:4,5]-pyrazino[1,2:1,6]pyrido[3,4-b]indole (CIPPCT) was presented. Energy-minimization, FT-MS and 2-D ROESY spectra defined CIPPCT taking Щ-like conformation and the intermolecular association drove CIPPCT forming finger ring like trimer. Images of transmission electron, scanning electron and atomic force microscopies consistently visualized that in aqueous solution of pH 6.7 and 10^{-10} M concentration CIPPCT generally assembled nano-particles of 9 - 67 nm in diameter. Mesoscale simulation demonstrated that a nano-particle of 9.4 nm in diameter contained 350 trimers. *In vivo* CIPPCT dose-dependently inhibited tumor growth of S180 mice. Elisa assay supported that CIPPCT concentration-dependently down-regulated serum uPA. The nano-particles of CIPPCT are capable of occurring in mouse plasma and adhering on HeLa cells, and nano-sized CIPPCT directly correlates the down-regulation of uPA with inhibition of tumor growth.

Keywords Intermolecular Association; Molecular Mechanism; Nano-particles; Nano-medicine; Anti-cancer; uPA

Table of contents entry

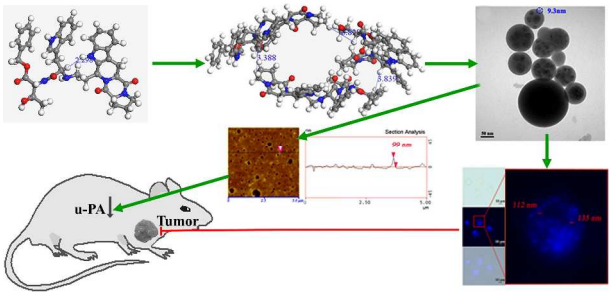

The mechanism of CIPPCT forming nano-particles capable of delivery in circulation and adhering on cancer cells was presented.

Introduction

The biological nano-systems have been perspectively viewed.[1-3] To prepare the nano-species and characterize the properties of the nano-materials various technologies have been developed,[4-11] which effectively promote the development of nano-medicine.[12-15] Regarding the nano-medicine, the progress of the nano-technology in the past decades mainly occurred in the preparation of drug delivery systems such as liposome.[16,17] Recently the self-assembly of single small molecule at nano-scale,[18,19] and the effect of the self-assembly of some small molecules on their biological properties attract intense interests.[20,21] Based on the advances, some bioactive small molecules capable of self-assembly have been used in the functionalization of metal surface,[22] in the crafting of functional biological materials,[23] and in the increase of the antiosteoporosis activity.[24] The physical and chemical mechanisms of small molecules forming nano-species, as well as the effect of the nano-species of small molecules on their pharmacological actions remain to be elucidated.

In various physiological processes related to tissue remodeling the plasminogen activator (PA) system is of importance. PA system consists of PAI-1/PAI-2 (the inhibitors of PA), urokinase-type plasminogen activator (uPA), the receptor of uPA (uPAR) and the plasminogen (the substrate of uPAR).[25] In respect of physiology, PAI-1 is a primary inhibitor of plasminogen activation in hemostasis and is one of the main regulators of the fibrinolytic system.[26]Abnormal expression of PAI-1 gene induces different disease including fibrosis, obesity, cancer and vascular disease.[27,28] In respect of carcinogenesis, up-regulation of PAI-1 gene results in the depression of tumors progression, and relates to a less aggressive phenotype of some cancers, presumably due to the inhibition of uPA activity.[27,29,30] The elevated level of PAI-1 in several primary malignant tumors, such as breast, gastric and ovarian cancers, as well as adenocarci-

nomas of lung, is considered as their marker.[27,28,31] On the other hand, high level of PAI-2 in tumour is associated with improved prognoses. In the presence of PAI-1, PAI-2 inhibits uPA, while in the presence of vitronectin, PAI-2 inhibits adherent cells. In inhibiting uPA elevated level of PAI-2 in tumour microenvironment out-competes PAI-1.[32]

Depending on the interactions of it with endogenous PAI-1, uPA exerts dual effects on tumor progression. In murine models, stable over-expression of uPA promotes the growth of colon tumors naturally expressing high PAI-1, but inhibits the growth of renal tumors naturally expressing low PAI-1.[33] In a variety of malignant tumours the over-expression of uPA and/or uPAR has been strongly correlated with poor prognosis. Impairing the function of uPA and/or uPAR, or inhibiting the expression of uPA and/or uPAR, limits the metastatic potential of many tumours.[34] Clinical and experimental evidences approve the significance of uPA and/or uPAR for a number of solid cancers, and the down-regulation of uPA and/or uPAR is considered a potential strategy in cancer therapy.[35, 36]

Perturbing the interaction between uPA and uPAR attracts some interests, and a few novel compounds were provided for inhibiting uPA. In a preliminary structure-activity exploration, amiloride analogs that inhibited uPA were dealt.[37] The N-nicotinonitrile derivatives that allege perturbing the interaction between uPA and uPAR failed to affect the expression of uPA.[38] Wide investigations are needed to successfully discover relevant lead compounds.

The course of discovering CIPPCT is depicted in Scheme 1. The (5aS,12S,14aS)-isomers of (5aS,12S/R,14aS)-5,14-dioxo-12-(2-aminoacid-N-ylethyl-1-yl)-1,2,3,5,5a,6,11,12,14,14a-decahydro-5H,14H-pyrolo[1,2:4,5]pyrazino[1,2:1,6]pyrido[3,4-b]indoles (DAPPP) were previously explored to be the inhibitors of urokinase.[39] Of (5aS,12S,14aS)-DAPPP analogs, 2-trptophan-N-ylethyl-1-yl derivative (CIPPC) more effectively antagonized the thrombolytic activity of urokinase, which provided a lead of u-PA inhibitor.[40] Of Trp-Trp-AA-OBzl, Trp-Trp-

Thr-OBzl possessed the highest anti-tumor activity, which provided a possible modification of CIPPC with Trp-Thr-OBzl.[41] In the formation of nano-particles WY3-56, an PAD4 inhibitor, the intermolecular π-π interactions was found to be essential, which provided an useful manner of designing nano-scale self-assembly.[42,43] Based on these a uPA inhibitor (5aS,12S,14aS)-5,14-dioxo-12-(2-tryptophanylthreo-nylbenzylester-N-ylethyl-1-yl)-1,2,3,5,5a,6,11,12,14,14a-decahydro-5H,14H-pyrolo[1,2:4,5]pyrazino[1,2:1,6]pyrido[3,4-b]indole (CIPPCT) was designed to investigate the mechanisms of forming nano-particles with FT-MS and 2-D ROESY spectra, to visualize the feature of the nano-particles with transmission electron, scanning electron and atomic force microscopies, to correlate the bioactivity with the nano-particles with the *in vitro* and the *in vivo* assays.

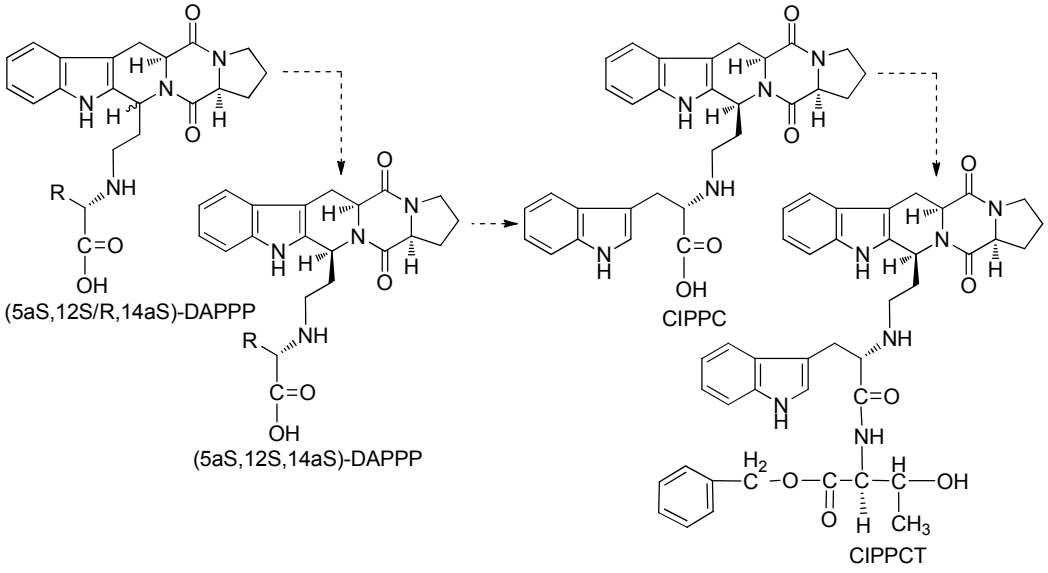

Scheme 1 Discovery course of CIPPCT

Experimental

Synthesis

To conveniently obtain CIPPCT a 5-step reaction sequence of Scheme 2 was used, which can be divided into steps 1-3 for preparing **3a**, and steps 4 and 5 for preparing CIPPCT.

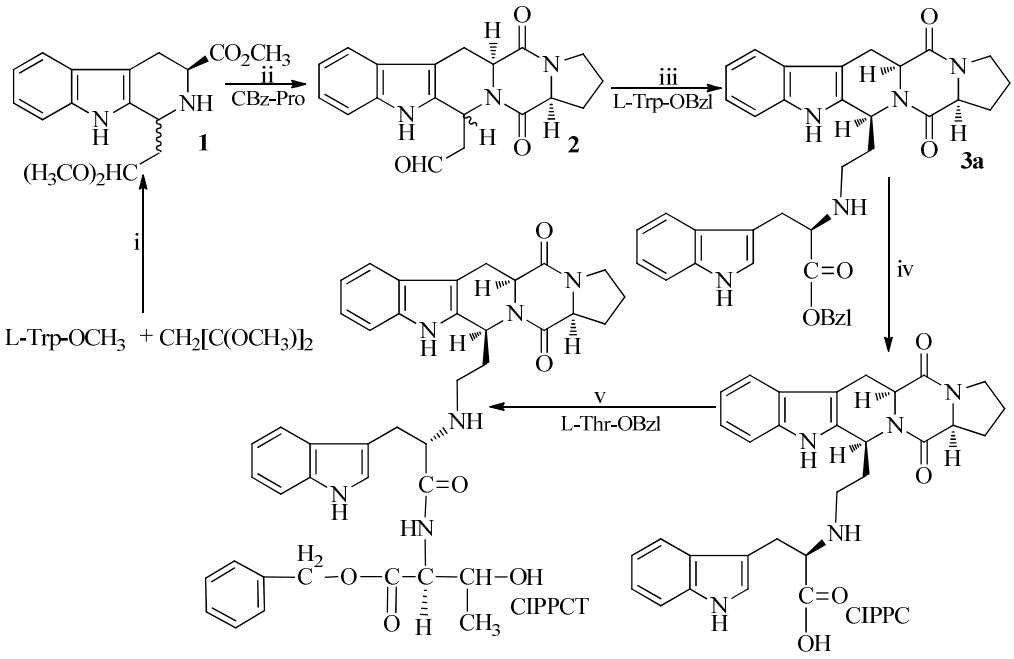

Scheme 2 Synthetic route of CICCPT

□) CH_3OH, hydrochloric acid, 45 ºC;□) $SOCl_2$, CH_2Cl_2, diisopropylamine; □) DMF,Et_3N, anhydrous Na_2SO_4, KBH_4, CH_3OH;□) DMF,DCC, anhydrous Na_2SO_4 ,N-methylmorpholine. The preparations of the compounds are described as follows and NMR spectrum are available in *Electronic Supplementary Information.*

Preparing 1-(2,2-dimethoxyethyl)-1,2,3,4-tetrahydrocarboline-3-carboxylic acid methyl ester (1). A suspension of 5.0 g l-tryptophan methyl ester (24.5 mmol) and 6.0 mL 1,1,3,3-tetramethoxypropane (23.6 mmol) in 50 mL CH_3OH was adjusted to pH 2 with hydrochloric acid (5M) and stirred at 45 ºC for 48 h. The reaction mixture was evaporated in vacuo to remove the solvent, the residue was diluted with 50 mL water and the formed solution was extracted with 30 mL ethyl acetate for 3 times. The extracts were combined and washed successively with 10% aqueous Na_2CO_3 (3 × 30 mL) and saturated aqueous NaCl (2 × 30 mL), then dried over anhydrous Na_2SO_4, filtered and concentrated in vacuo to provide **1**. ESI-MS (m/z): 319 $[M+H]^+$.

Preparing (5aS,12S/R,14aS)-5,14-dioxo-12-cabonylmethyl-1,2,3,5,5a,6,11,12, 14,14a-decahydro-5H,14H-pyrolo[1,2:4,5]pyrazino[1,2:1,6]pyrido [3,4-b]indole (2). To 5.0 g CBz-L-Pro (14.8 mmol) 50 mL $SOCl_2$ was added dropwise and the reaction mixture was heated for 5-h reflux. The mixture was concentrated in vacuo to remove excess $SOCl_2$. The residue was treated with 30 mL ether to provide CBz- protected prolinyl chloride as colorless powder, to which a solution of 3.2 g 1-(2,2- dimethoxyethyl)-1,2,3,4-tetrahydrocarboline-3-carboxylic acid methyl ester (**1**, 10 mmol) in 50 mL CH_2Cl_2 was added at 0 ºC and stirred for 0.5 h. The reaction mixture was adjusted to pH 9 with diisopropylamine and stirred at room temperature for 24 h. The reaction mixture was concentrated in vacuo, the residue was dissolved in 150 mL acetone, and the solution was treated with 200 mg p-TsOH. After stirring at 45 ºC for 1 h, the reaction mixture was treated with 5 mL Et_3N, concentrated in vacuo, the residue was purified on column chromatography ($CHCl_3$/CH_3OH, 40:1), the interesting fraction was evaporated in vacuo, and the residue was recrystallized from acetone to provide 1.5g (29%) of the title compound. ESI-MS (m/z): 338 $[M+H]^+$.

Preparing (5aS,12S,14aS)- and (5aS,12R,14aS)-5,14-dioxo-12-(2-tryptophan- benzylester-N-ylethyl-1-yl)-1,2,3,5,-5a,6,11,12,14,14a-decahydro-5H,14H-pyrolo[1,2:4,5]pyrazino-[1,2:1,6]pyrido[3,4-b]indoles (3a and 3b). To a solution of 2.3 g (5aS,12S/R,14aS)-5,14-dioxo-12-cabonylmethyl-1,2,3,5,5a, 6,11, 12, 14,14a-deca- hydro-5H,14H-pyrolo[1,2:4,5]pyrazino-[1,2:1,6]pyrido[3,4-b]indole (**2**, 6.8 mmol) in 10 mL DMF was added 2.4 g HCl·Trp-OBzl (6.8 mmol), 1.5 mL Et_3N and 6 g anhydrous Na_2SO_4. The reaction mixture was stirred at room temperature for 3 h, to a solution of 1 g KBH_4 (18.4 mmol) in 10 mL CH_3OH was added, and stirred for another 1 h. The reaction mixture was evaporated in vacuo, and the residue was dissolved with 40 mL ethyl acetate and 20 mL deionized water. The two-phase solution was

treated with 2 mL hydrochloric acid (5 M) to decompose excess KBH_4, and adjusted to pH 9 with aqua ammonia NH_3 (5 M). The ethyl acetate phase was separated, and the aqueous phase was extracted with ethyl acetate (3 × 40 mL). The combined ethyl acetate phases were washed with 40 mL saturated aqueous NaCl, dried with anhydrous Na_2SO_4, filtered and concentrated in vacuo. The residue was purified and separated on column chromatography ($CHCl_3$/CH_3OH, 30:1) to give 1.3 g (61%) **3a** and 1.5 g (71%) **3b**.

3a: FT-MS (m/z): 615.2830 $[M]^+$; mp:175 -176 °C; ^{1}HNMR (300MHz, $CDCl_3$): δ = 8.223 (s, 1H), 7.756-7.584 (dd, *J* = 7.5 Hz, *J* = 7.5Hz, 2H), 7.494 - 7.411 (m, 3H), 7.411(m, 3H), 7.386 - 7.317 (m, 5H), 7.155 - 7.149 (m, 3H), 7.05 (m, 1H), 6.084 - 6.057 (d, *J* = 8,1 Hz, 1H), 5.538 - 5.488 (q, *J* = 4.8 Hz, 5.1Hz, 1H), 5.216 (s, 2H), 4.174 (m, 1H), 4.106 (m, 1H), 4.004 - 3.988(d, *J* = 4.8Hz, 1H), 3.559 - 3.542 (m, 1H), 3.434 - 3.288(td, *J* = 5.1Hz, *J* = 3.0 Hz, *J* = 3.0 Hz, 2H), 2.959 - 2.910 (m, 2H), 2.886 - 2.757 (m, 2H), 2.743 - 2.655 (m, 1H), 2.466 - 2.376 (m, 1H), 2.318 - 2.198 (m, 2H), 2.098 - 1.913 (m, 2H); ^{13}C NMR (75 MHz, $CDCl_3$): δ = 173.86, 169.48, 165.90, 165.83, 156.14, 136.34, 135.96, 135.71, 135.38, 133.96, 133.53, 129.60, 128.61, 128.34, 128.21, 126.99, 126.10, 125.66, 123.71, 122.59, 122.13, 121.39, 120.30, 120.12, 120.01, 119.41, 118.88, 118.17, 117.66, 115.44, 112.07, 111.83, 111.43, 111.23, 106.39, 105.70, 66.68, 62.21, 59.34, 59.19, 58.89, 57.40, 56.95, 50.28, 49.14, 46.24, 45.37, 44.46, 40.43, 35.44, 29.51, 28.64, 28.54, 23.24, 23.12, 21.41, 21.23, 10.00; IR (KBr): 3308, 2978, 2954, 2880, 1659, 1454, 1398, 1335, 1236, 1096, 745 cm^{-1}. In ROESY 2D NMR spectrum a positive NOE signal between 5aS-H and 12-H was observed.

3b: FT-MS (m/z): 615.2845 $[M]^+$; mp:105 -106 °C; ^{1}HNMR (300 MHz, $CDCl_3$): δ = 11.087 (s, 1H), 10.677 (s, 1H), 7.458 - 7.404 (dd, *J* = 4.8Hz, *J* = 5.2Hz, 2H), 7.295 -7.250 (m, 7H), 7.075 - 6.935 (m, 4H), 6.068 - 6.040 (dd, *J* = 1.8Hz, *J* = 1.8Hz, 1H), 5.216 - 5.134(dt, *J* = 7.8Hz, *J* =

7.8Hz, 2H), 4.765 - 4.734 (dd, *J* = 2.7Hz, *J* = 2.4Hz, 1H), 4.258 - 4.235 (d, *J* = 6.9Hz, 1H), 4.193 - 4.138(m, 2H), 3.806 - 3.790 (m, 1H), 3.428 - 3.388(dd, *J* = 2.7Hz, *J* = 2.7Hz, 2H), 3.333 (m, 4H) 3.012 - 2.982 (m, 2H), 2.875 - 2.727 (m, 1H), 2.407 - 2.361(t, *J* = 6.9Hz, *J* = 6.9Hz, 1H), 2.226 - 2.209 (t, *J* = 2.4Hz, 2.7Hz, 1H), 2.176 - 2.124 (m, 1H), 1.934 - 1.918 (m, 1H), 1.855 - 1.788 (m, 2H); ^{13}C NMR (75 MHz, $CDCl_3$): δ = 174.03, 165.51, 164.42, 136.66, 136.55, 136.29, 135.99, 133.66, 128.81, 128.29, 127.82, 127.13, 126.58, 121.68, 121.14, 119.23, 118.82, 118.26, 118.02, 111.61, 111.25, 106.00, 105.56, 66.04, 58.77, 53.54, 52.90, 46.90, 46.40, 45.06, 29.93, 28.63, 25.22, 21.46; IR (KBr): 3251, 3233, 2957, 2930, 2857, 1659, 1454, 1398, 1150, 748 cm^{-1}. In ROESY 2D NMR spectrum no NOE signal between 5aS-H and 12-H was observed.

Preparing (5aS,12S,14aS)-5,14-dioxo-12-(2-tryptophan-N-ylethyl-1-yl)-1,2,3,5,5a, 6,11,12,14,14a-decahydro-5H,14H-pyrolo[1,2:4,5]pyrazino[1,2:1,6]pyrido[3,4-b]- indoles (CIPPC). To a solution of 1.3 g (5aS,12S,14aS)-5,14-dioxo-12-(2-trypto- phanbenzylester-nylethyl-1-yl)-1,2,3,5,-5a,6,11,12,14,14a-decahydro-5H,14H-pyrolo- [1,2:4,5]pyrazino[1,2:1,6]-pyrido[3,4-b]indoles (**3a**, 2.1 mmol) in 5 mL methanol aqueous NaOH (4 M) was added dropwise to adjust pH 12, and the reaction mixture was stirred at room temperature for 2 h. The reaction mixture was adjusted pH 5 with hydrochloric acid (2 M), evaporated under vacuo, and the residue was purified on silica gel column to provide 863 mg (90%) of CIPPC. ESI –MS (m/z): 526 $[M+H]^+$; ^{1}H NMR (400 MHz, DM*S*O), δ(ppm) = 11.27 (*s*, 1H), 10.86 (*s*, 1H), 7.54 (*dd, J* = 7.6, *J* = 7.6 Hz, 2H), 7.33 (m, 2H), 7.13 (*s*, 1H), 7.06 (*s*, 2H), 6.92 (t, ***J*** = 7.2 Hz, 1H), 5.38 (*s*, 1H), 4.50 (*s*, 1H), 4.29 (m, 2H), 3.45 - 3.34 (m, 4H), 3.24 (*s*, 1H), 3.15 (m, 2H), 2.83 (m, 1H), 2.51 (*s*, 1H), 2.22 (*s*, 1H), 1.98 - 1.79 (m, 5H). ^{13}C NMR (100 MHz, DM*S*O), δ(ppm)= 171.11, 170.44, 165.55, 136.34, 136.00, 133.98, 125.95, 124.11, 121.65, 118.64, 118.47, 118.19, 111,71, 111.47, 109.49, 105.53, 101.53, 63.10, 62.17, 58.69, 56.32, 52.87, 49.42, 45.03, 43.18, 40.37, 40.16, 39.95, 36.27, 34.60, 28.21, 26.75, 22.93, 21.33. IR (KBr): 3390.86, 3269.34, 3113,

3057, 3014, 2954, 2933, 2877, 1640, 1465, 1303, 1130, 1103, 1008, 762, 702 cm^{-1}.

Preparing (5aS,12S,14aS)-5,14-dioxo-12-(2-tryptophanyl-threoninebenzylester-N-ylethyl-1-yl)-1,2,3,5,-5a,6,11,12,14,14a-decahydro-5H,14H-pyrolo[1,2:4,5]pyrazino[1,2:1,6]pyrido-[3,4-b]indoles (CIPPCT). To a solution of 120 mg (0.23 mmol) CIPPC and 77 mg (0.23 mmol) Thr-OBzl in 15 mL anhydrous DMF 100 mg (0.46 mmol) DCC and 30 mg anhydrous Na_2SO_4 were added. The reaction mixture was adjusted pH 9 with N-methylmorpholine, and at room temperature for 1 h. The reaction mixture was evaporated under vacuo, the residue was dissolved in 20 mL ethyl acetate, the solution was washed with 10% aqueous Na_2CO_3 (15 mL × 3) and dried with anhydrous Na_2SO_4. After filtration the filtrate was evaporated under vacuo, and the residue was purified on silica gel column to provide 129 mg (78%) CIPPCT as yellowness powders. Mp 127 - 128 ºC. $[\alpha]_D^{20}$ = -191 (c = 0.6, CH_2Cl_2). FT-MS(m/z): 717.33161 $[M+H]^+$. ^1H NMR (300 MHz, $CDCl_3$): δ(ppm) = 8.27 (s, 1H), 8.02 (t, *J* = 5.4 Hz, 1H), 7.974 (d, *J* = 7.8 Hz, 1H), 7.464 (m, 2H), 7.364 (m, 5H), 7.319 (d, *J* = 2.1 Hz, 1H), 7.173 (m, 2H), 7.120 (m, 1H), 6.128 (s, 1H), 5.186 (s, 2H), 4.264 (d, *J* = 6.6 Hz, 1H), 4.240 (m, 1H), 4.203 (d, *J* = 6.6 Hz, 1H), 4.040 (d, *J* = 4.8 Hz, 1H), 3.964 (m, 1H), 3.879 (dd, *J* = 5.1 Hz, *J* = 7.2 Hz, 1H), 3.768 (m, 1H), 3.630 (m, 2H), 3.490 (m, 1H), 3.350 (m, *J* = 5.1 Hz, 1H), 2.900 (m, 2H), 2.511 (m, 2H), 2.467 (m, 2H), 2.241 (m, 1H), 2.005 (m, 3H), 1.241 (dd, *J* = 4.2 Hz, *J* = 7.2 Hz, 3H). ^{13}C NMR (75 MHz, $CDCl_3$): δ(ppm) = 171.1, 170.7, 165.8, 162.6, 136.5, 135.6, 135.2, 133.8, 128.6, 128.5, 128.4, 127.6,127.0, 125.8, 124.9, 122.5, 121.8, 119.9, 119.8, 119.4, 117.9, 112.0, 111.4, 105.7, 68.2, 67.3, 65.3, 60.7, 60.4, 59.3, 57.4, 48.0, 46.1, 45.2, 42.8, 36.5, 35.1, 31.4, 29.7, 29.6, 28.6, 23.3, 21.0, 20.8, 20.0, 14.2, 8.6. IR (KBr): 3387, 3325, 2974, 2928, 2884, 1742, 1649, 1520, 1454, 1402, 1339, 1196, 1111, 745, 845 cm^{-1}.

Generation of energy-minimized conformation

CIPPCT was sketched in ChemDraw 10.0, converted to 3D conformation in Chem3D 10.0 and then energy minimized in Discovery Studio 3.5 with MMFF force field. The energy-minimized conformation was utilized as the starting conformation for conformation generation. The energy-minimized conformations of CIPPCT were sampled in the whole conformational space via systematic search and BEST methods in Discovery Studio 3.5. Both of the systematic search and BEST methods were practiced with SMART minimizer using CHARMm force field. The energy threshold was set to 20kcal/mol at 300 K. The maximum minimization steps were set to 200 and the minimization RMS gradient was set to 0.1 Å. The maximum generated conformations were set to 255 with a RMSD cutoff 0.2 Å.

Measuring two-dimensional ROESY spectra

One-dimensional ^{1}H NMR spectrum of 10 mg CIPPCT in 0.5 mL deuteron dimethyl sulfoxide (DMSO-d6) was measured on a Bruker 800MHz spectrometer. The probe temperature was regulated to 298 K. By using a simple pulse-acquire sequence zg30 the spectra were recorded. To ensure full relaxation of the ^{1}H resonances typical acquisition parameters consisted of 64 K points covering a sweep width of 16447 Hz, a pulse width (pw90) of 8.63 μs and a total repetition time of 24 s were used. Before Fourier Transformation the digital zero filling to 64 K and a 0.3 Hz exponential function were applied to the FID. The resonance at 2.5 ppm presented impurity (CD_2HSOCD_2H) in the residual solvents, and tetramethylsilane (TMS) was used as internal reference. Standard absorptive two-dimensional ^{1}H-^{1}H chemical shift correlation spectra (COSY) were tested with the same spectrometer. Each spectrum consisted of a matrix of 2 K (F2) by 0.5 K (F1) covering a sweep width of 9615.4 Hz. Before Fourier Transformation, the matrix was zero filled to 1 K by 1 K and the standard sinebell apodization functions were applied in both dimensions. Two-dimensional ROESY experiments were carried out in the phase-

sensitive mode by using the same spectrometer. Each spectrum consisted of a matrix of 2 K (F2) by 1 K (F1) and covered a sweep width of 9615.4 Hz. Spectra were obtained using spin-lock mixing periods of 200 ms. Before Fourier Transformation, the matrix was zero filled to 1 K by 1 K and qsine apodization functions were applied in both dimensions.

Measuring FT-MS spectra

ESI mass spectra of CIPPCT were measured on a solariX FT-ICR mass spectrometer (Bruker Daltonics, Billerica, MA, USA) consisted of an ESI/MALDI dual ion source and a 9.4 T superconductive magnet. The measurements were performed with the positive Maldi ion mode. The ion source was a Smart-beam-II laser (wavelength, 355 nm; focus setting, 'medium'; repetition rate, 1000 Hz). QCID mass was set to 2150.98172 m/z, and the isolation window was 5 m/z. Data were collected by using solariXcontrol software. Spectral data were processed with Data Analysis software (Bruker Daltonics).

Measuring TEM images

Shape and size measurementns of CIPPCT nanospecies were performed with transmission electron microscopy (TEM; JSM-6360 LV, JEOL, Tokyo, Japan). An aqueous solution of CIPPCT (pH 6.7, 10^{-10} M) was dripped onto a formvar-coated copper grid, to which a drop of anhydrous ethanol was added to promote the removal of water. The grid was allowed to dry thoroughly in air and then was heated at 35 °C for 24 h. The copper grids were viewed under TEM. The shape and size distributions of the nanospecies were determined by counting >100 species in randomly selected regions on the copper grid. All of the determinations were carried out on triplicate grids and at 80 kV (the electron beam accelerating voltage). Images were recorded on an imaging plate (Gatan Bioscan Camera Model 1792, Pleasanton, CA, USA) with 20 eV energy windows at 6000 - 400,000× and were digitally enlarged.

Measuring SEM images

The shape and size of lyophilized powders of CIPPCT (from a solution of CIPPCT in ultrapure water) were measured by scanning electron microscopy (SEM, JEM-1230, JEOL, Tokyo, Japan) at 50 kV. The lyophilized powders were attached to a copper plate with double-sided tape (Euromedex, Strasbourg, France). The specimens were coated with 20 nm gold-palladium using a Joel JFC-1600 Auto Fine Coater. The coater was operated at 15 kV, 30 mA, and 200 mTorr (argon) for 60 s. The shape and size distributions of the lyophilized powders of CIPPCT were measured by examining >100 particles in randomly selected regions on the SEM alloy. All measurements were performed on triplicate copper plates. Images were recorded on an imaging plate (Gatan Bioscan Camera Model1792) with 20 eV energy windows at 100 - 10,000 ×, and were digitally enlarged.

Measuring AFM images

Atomic force microscopy (AFM) images of contact mode were recorded on a Nanoscope 3D AFM (Veeco Metrology, Santa Barbara, CA, USA) under ambient conditions. Samples of CIPPCT in water (pH 6.7, 10^{-10} M) were used for recording the images.

Theoretically predicting nanoparticle size

The mesoscale simulation software was used to perform the calculation, and to predict how many trimers of CIPPCT can construct the smallest nanoparticle revealed by TEM. Discover module of the Materials Studio software was used for the simulation. CIPPCT molecule was built and optimized simply in the Visualizer window. “Beads” were constructed from atomistic simulations and placed at the center-of-mass of groups of atoms corresponding to particular parts of CIPPCT molecule.

***In vitro* anti-proliferation assay**

In vitro cell viability assays were carried out by using 96-well microtiter culture plates and MTT [3-(4,5-dimethylthiazol-2-yl)-2,5-diphenyltetrazolium bromide] staining, according to the standard procedures. HL-60, HT-29, HeLa, SW480 and HepG2 cells (5×10^3 cells/well) were grown in RPMI-1640 or DMEM medium [containing 10% (v/v) fetal calf serum, 60 μg/mL penicillin, and 100 μg/mL streptomycin]. Stock solutions of CIPPCT were prepared in DMSO and diluted with culture medium to desired concentration. Cultures were propagated at 37 °C in a humidified atmosphere (with 5% CO_2) for 24 h, and then CIPPCT was added (final concentrations were 0, 1, 5 10, 25, 50 and 100 μM). After 48 h of treatment, MTT solution was added (5 μg/mL; 25 μL/well), and cells were incubated for an additional 4 h. After adding 100 μL of DMSO to dissolve the MTT-formazan product, the optical density was measured at 570 nm by a microplate reader (n = 6).

***In vivo* anti-tumor assay** Following the protocol reviewed and approved by the ethics committee of Capital Medical University, the investigations were performed. The committee assures that the welfare of mice was maintained in accordance with the requirements of the animal welfare act. Male ICR mice (22 ± 2g, purchased from Capital Medical University) were maintained at 21 °C with a natural day/night cycle in a conventional animal colony. Mice were 10 weeks old at the beginning of the experiment. S180 ascites tumor cells were subcutaneously injected to form solid tumors. To initiate subcutaneous tumors, cells obtained in ascitic form from tumor-bearing mice were serially transplanted once per week. Subcutaneous tumors were implanted under the skin at the right armpit by injecting 0.2 mL of NS (normal saline) containing 1×10^7 viable tumor cells. Twenty-four hours after implantation, mice were randomly divided into treatment, positive control and vehicle control groups (7 per group). For treatment groups CIPPCT in 0.2 mL of

0.3% carmellose sodium (CMC-Na) was orally administered at 4.0, 0.8 and 0.16 μmol/kg of dose. For positive control group doxorubicin in NS was intraperitoneally injected at 2 μmol/kg of dose. For vehicle control 0.2 mL of CMC-Na (0.3%, negative control) was orally given. Oral administrations for treating groups or for vehicle control or intraperitoneal injections for positive control were given every day for 7 days. Mice were weighed daily. Twenty-four hours after the last administration, mice were weighed, sampled blood from eyes, sacrificed by ether anesthesia, and dissected to immediately obtain and weigh the tumor and organ samples.

uPA Elisa assay

uPA level in the serum of S180 mice tread with CIPPCT at 4, 0.8 and 0.15 μmol/kg of doses was measured by enzyme immunoassay according to the manufacturer's instructions (mouse uPA ELISA kit, Uscn Life Science Inc. Wuhan). In brief, 24 h after the last administration mouse blood was collected in 3.8% aqueous solution of sodium citrate from eyes, kept at room temperature for 30 min, centrifuged at 3000 rpm for 20 min and the separated serum was kept at -20 ºC before use. In ELISA assay, murine monoclonal antibody specific for uPA was coated on the 96-well microplate. Each standard and serum sample was added to the plate and incubated. After washing away unbound proteins, enzyme-linked antibody specific for uPA was added to the wells. Absorbency was measured at 492 nm. The detection limit was 100 pg/mL. All samples were run in duplicates. The variations of intra and inter assays were less than 10%.

Results and discussion

Energy-minimization and Ш-like conformation

A Ш-like conformation of CIPPCT was generated in computer-assisted molecular modeling. The systematic search method produced 30 conformations, and the BEST method produced 203 conformations. The 233 generated conformations were visually examined and the conformation having the lowest free energy was selected. This conformation has a -35.06 kcal/mol relative

energy to the starting conformation. In respect of the steric relationship between pyrolo[1,2:4,5]pyrazino[1,2:1,6]pyrido[3,4-b]indole, trptrophan and benzyl moieties, CIPPCT had a Щ-like conformation, in which the distance from pyrrole-H of pyrolo[1,2:4,5]pyrazino-[1,2:1,6]pyrido[3,4-b]indole moiety to α-H of trptrophan moiety was 2.298 Å, which was reflected by cross-peak a in the ROESY 2D NMR spectrum (see Fig. 2b).

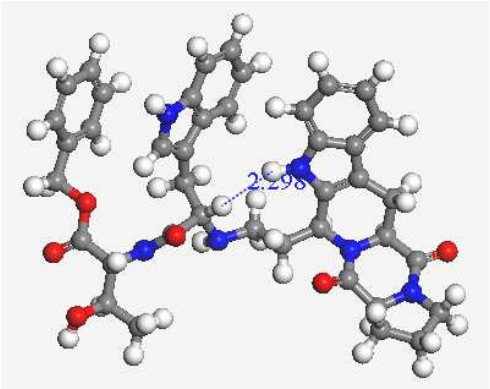

Figure 1 A Щ-like conformation, the energy-minimized conformation.

FT-MS spectroscopy and trimer

The intermolecular association of CIPPCT was explained with FT-MS spectrum (Figure 2a). This spectrum gave three interesting ions. The ion 717.33161 (bearing one positive charge) represents the mass of a CIPPCT monomer (theoretical value: 716.3322) plus H. The ion 1433.66550 (bearing one positive charge) represents the mass of a CIPPCT dimer (theoretical value: 1432.6644) plus H. The ion 2149.96613 (bearing one positive charge) represents the mass of a CIPPCT trimer (theoretical value: 2148.9966) plus H. The monomer ion was characterized by the highest peak, among the 3 ions. To clarify the correlation of the momomer, the dimer and the trimer a qCID spectrum was measured and inserted into Figure 2a. The qCID spectrum demonstrated that the dimer and the monomer were derived from the fragmentation of the trimer under FT-MS conditions. Therefore the spectra support an interpretation that the intermolecular association leads to trimerization and in aqueous CIPPCT exists as trimer.

ROESY 2D NMR spectrum and trimerization manner

The manner of the intermolecular association was identified with ROESY 2D NMR spectrum. In Figure 2b the ROESY related three cross-peaks were labeled with blue circles. Of three cross-peaks, the cross-peak a was assigned for the interaction of pyrrole-H in pyrolo[1,2:4,5]pyrazino-[1,2:1,6]pyrido[3,4-b]indole moiety with the α-H of trptrophan moiety, and reflected the steric relationship of two intramolecular H according to the low energy conformation of Figure 1. The cross-peak b was assigned for the interaction of the H of CH_2 in benzyl moiety with the 13-H in pyrolo[1,2:4,5]pyrazino[1,2:1,6]pyrido[3,4-b]indole moiety, according to the low energy conformation of Figure 1 this interaction can only result from two intermolecular H. The cross-peak c was assigned for the interaction of the 19-H in pyrolo[1,2:4,5]pyrazino[1,2:1,6]pyrido-[3,4-b]indole moiety with the α-H of threonine moiety, according to the low energy conformation defined in Figure 1 this interaction can also only result from two intermolecular H. To fit the requirements of cross-peaks b and c three CIPPCT molecules could associate in a manner of Figure 2c and form a finger ring like species. The data of NMR and MS together supported an interpretation that CIPPCT existed as finger ring like trimer.

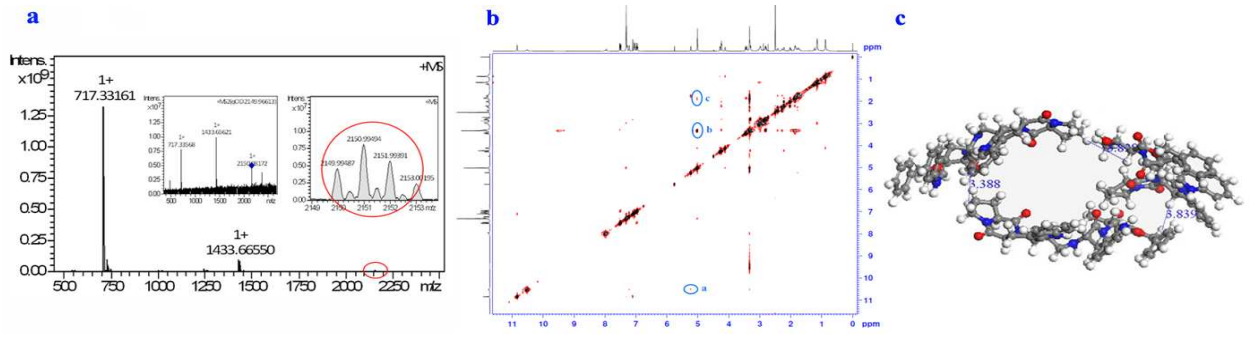

Figure 2. a) Ion peak in the FT-MS spectrum supporting trimerization of CIPPCT (bearing one positive charges, 2149.96613). The inset shows a qCID spectrum, indicating that monomers and dimers are resulted from fragmentation of the trimer under FT-MS conditions. b) ROESY 2D NMR spectrum: three cross-peaks indicating the intermolecular associations of CIPPCT (labeled

with blue circles). c) Finger ring like trimer of CIPPCT, deduced from the ROESY 2D NMR and FT-MS spectra, in which the distances of the hydrogen in the cross-peaks b and c were indicated.

TEM, SEM, AFM and nano-particles

Nano-structure was shown with TEM**,** SEM and AFM images. TEM images of Figure 3a explored that in aqueous solution of pH 6.7 and 10^{-10} M concentration CIPPCT formed nano-particles of 9 - 194 nm in diameter, and the diameter of most particles was less than 125 nm. SEM images of Figure 3b explored that the precipitates from the aqueous solution of pH 6.7 and 10^{-10} M concentration were the nano-particles of 27 - 67 nm in diameter, and the diameter of most particles was less than 47 nm. AFM images of Figures 3c and 3d explored that the precipitates from an aqueous solution of pH 6.7 and 10^{-10} M concentration were nano-particles of 74 - 79 nm in diameter. All images consistently visualized that when an aqueous solution of 10^{-10} M of CIPPCT was administered the nano-particle was its basic structure, and implied that in aqueous solution its timers can spontaneously assemble to nano-particles due to intermolecular association addressed by FT-MS and ROESY 2D NMR spectra.

Theoretical prediction and trimer number in nanoparticle

Mesoscale simulation predicted that the trimers of CIPPCT spontaneously formed nanoparticles and a nanoparticle of 9.4 nm in diameter contained 350 trimers (Figure 3e). As seen in Figure 3a, the smallest nano-particle had a diameter of 9.3 nm. The consistency of the theoretically predicted nanoparticle with the experimentally tested nanoparticle emphasized the utility of the theoretical prediction. Besides, this prediction provided an approach to quantitatively estimate the number of the trimers for an optional nano-particle.

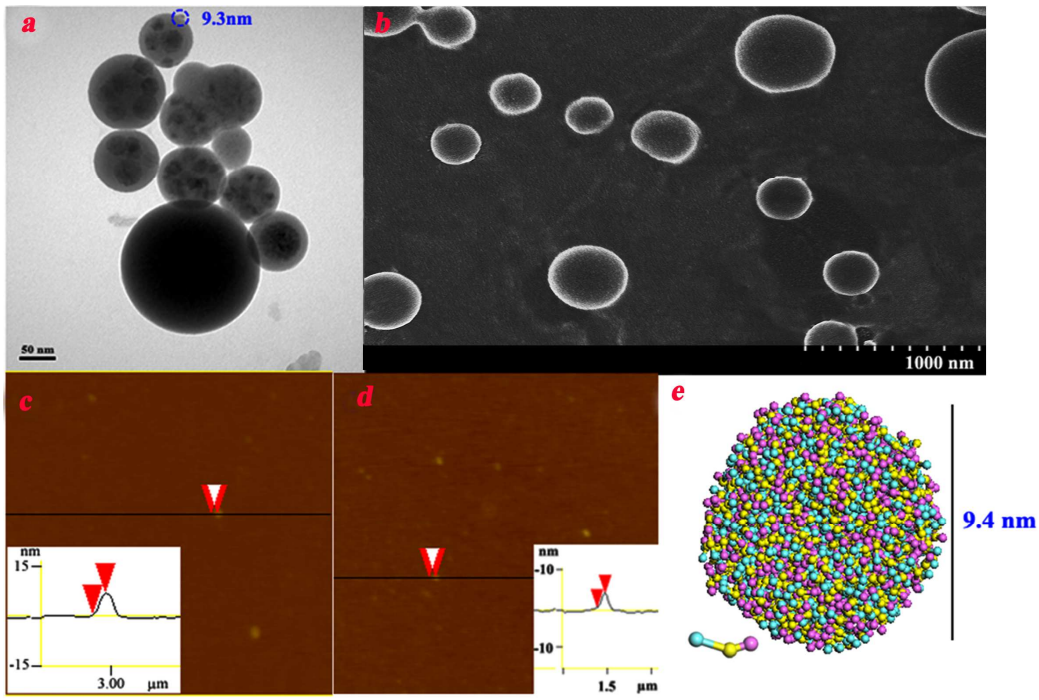

Figure 3 TEM, SEM and AFM images as well as mesoscale simulation software assisted calculation of the nano-particles of CIPPCT. (a) TEM images of CIPPCT in pH 6.7 and 10^{-10} M aqueous solution. (b). SEM images of powders of CIPPCT precipitated from pH 6.7 and 10^{-10} M aqueous solution. (c,d) AFM images of CIPPCT precipitated from pH 6.7 and 10^{-10} M aqueous solution. (e) Mesoscale simulation software assisted calculation of the structure of CIPPCT nano-particles. CIPPCT were divided into three beads. The green, yellow and pink beads represented pyrolo[1,2:4,5]pyrazino[1,2:1,6]pyrido[3,4-b]indole, tryptophan and threonine moieties, respectively.

IC_{50} for inhibiting cancer cell proliferation

The cytotoxicity of CIPPCT to HL60, HT29, HeLa, SW480 and HepG2 cells was examined with MTT method, represented with IC_{50} values and are shown in Figure 4a. As seen, in the MTT assays the IC_{50} values in inhibiting HeLa and SW480 cells were more than 100 μM, the IC_{50} value in inhibiting HepG2 cells was more than 60 μM, the IC_{50} value in inhibiting HT29 cells was more than 20 μM, and the IC_{50} value in inhibiting HL60 cells was more than 10 μM. The

relative higher IC_{50} values suggest CIPPCT had low cytotoxicity and should not be a cytotoxic agent.

Dose-dependent inhibition for tumor growth

The *in vivo* anti-tumor activity of CIPPCT was assayed on S180 mouse model, represented with tumor weight, and are shown in Figure 4b. The assays led CIPPCT to exhibiting an orally dose-dependent inhibition and to having an effective dose of 0.16 μmol/kg low. In respect of 4 μmol/kg oral dose, CIPPCT had the same efficacy as 2 μmol/kg of intraperitoneally injected doxorubicin, suggesting oral administration of CIPPCT can offer desirable therapeutic effectiveness.

uPA levels in serum of mice treated with CIPPCT

The anti-tumor mechanism of CIPPCT was explained with ELISA experiments and the uPA levels in the serum treated with 4.0, 0.8 and 0.16 μmol/kg of oral CIPPCT are shown in Figure 4c. In a variety of malignant tumours the over-expression of uPA has been strongly correlated with poor prognosis. Experimental evidences approved that the down-regulation of uPA was considered a potential strategy in cancer therapy.[11, 12] CIPPCT dose-dependently decreased uPA levels in the serum of mice, reflecting CIPPCT dose-dependently down-regulated uPA expression and suggesting by targeting uPA CIPPCT inhibited tumor growth.

AFM of CIPPCT nano-particles in mouse plasma

To visualize the morphological feature of CIPPCT in the blood, AFM test was performed on a Nanoscope 3D AFM (Veeco). By using contact mode, the images of mouse plasma alone (negative control) and CIPPCT in mouse plasma (10^{-10} M, pH7.4) were recorded. The images in Figure 4e show that in mouse plasma the nano-particles of CIPPCT are 99 nm in high. While the mouse plasma gives no any comparable nano-particle (Fig. 4d).

Time-dependent adherence of CIPPCT nano-particles onto the surface of HeLa cells

With 282 nm excitation wave CIPPCT can emit blue fluorescence of 418 nm, and this spectrum property was used to monitor the nano-particles. In this case CIPPCT nano-particles on cell surface were characterized by fluorescence images (Figure 4f). As seen, when tumorigenic cells, HepG2, were treated with CIPPCT (10^{-10} M) the blue fluorescent nano-particles of 100-135 nm in diameter steadily increased as the treatment time lengthened from 15 min to 240 min, particularly beyond 60 min.

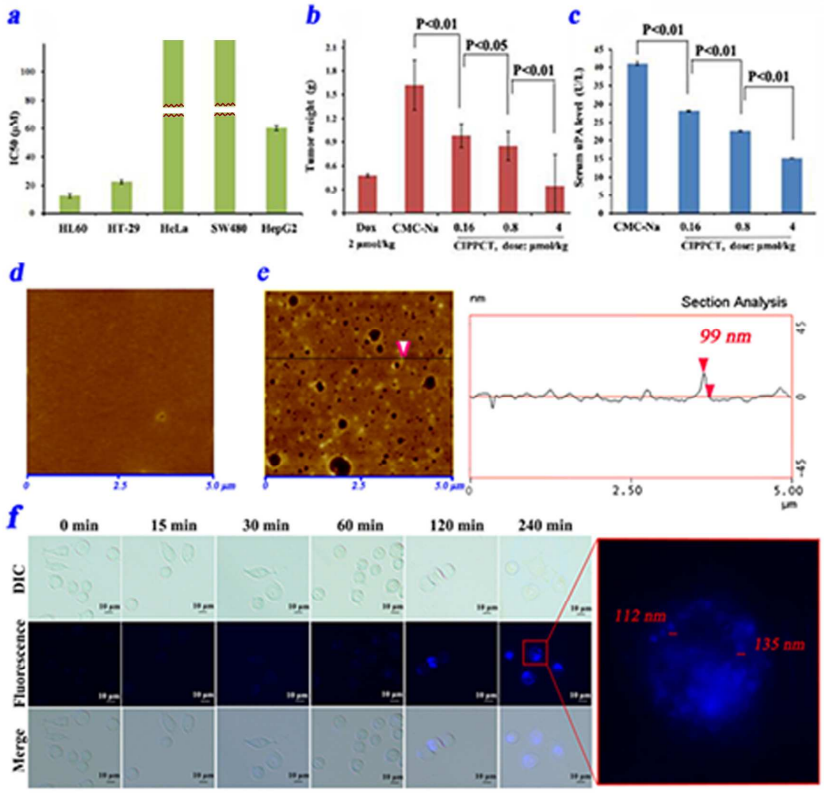

Figure 4 CIPPCT possessed bioactivity on molecular, cell and animal models. a) IC_{50} of CIPPCT in inhibiting cancer cell proliferation, n = 6; b) *In vivo* CIPPCT dose-dependently inhibiting tumor growth, n = 10; c) *In vivo* CIPPCT dose-dependently decreasing serum uPA level, n = 10; d) AFM image of mouse plasma alone; e) AFM image of nano-particles of CIPPCT in mouse plasma; f) Fluorescence images demonstrating the time-dependent adherence of CIPPCT nano-particles onto the surface of HeLa cells.

Conclusion

In conclusions, with energy-minimization simulation, FT-MS spectra, ^{1}H NMR Noesy spectra, and images of TEM, SEM and AFM, the chemical and physical mechanism of CIPPCT forming nano-particles could be clarified. Elisa, anti-proliferation and tumor growth assays evidenced that down-regulating uPA was the pharmacological mechanism of CIPPCT inhibiting tumor growth, and benefited the increase of anti-tumor activity and decrease the cytotoxicity.

Contribution of Each Author

The contribution of each author made to the manuscript Mechanism of forming trimer, self-assembling nano-particle and inhibiting tumor growth of small molecule CIPPCT is as followings:Chemical synthesis, In vivo anti-tumor assay and uPA Elisa assay: Dr. Fengxiang Du;

Mesoscale Simulation and figures: Dr. Xiaoyi Zhang

In vitro anti-proliferation assay: Dr. Shan Li

MS,NMR and AFM data testing: Yaonan Wang, Meiqing Zheng and Shurui Zhao;

MS/NMR data collection and interpretation: Dr. Yuji Wang;

Literature search: Dr. Jianhui Wu;

TEM and SEM measuring: Dr. Lin Gui;

Experimental design: Dr. Ming Zhao;

Research guidance and paper writing: Dr. Shiqi Peng.

Acknowledgements

This work was supported by the Beijing area major laboratory of peptide and small molecular drugs, by PHR (IHLB), by the Natural Science Foundation (81373265 and 81270046) Beijing

Natural Science Foundation (7112016 and 7132032) and by Beijing Municipal Science & Technology Commission (2014).

Electronic Supplementary Information (ESI) available: [NMR spectra of CIPPCT were included.]. See DOI: 10.1039/b000000x/

Notes

The authors declare no competing financial interest.

References

1 W.Guannan, S.Xingguang, The synthesis and bio-applications of magnetic and fluorescent bifunctional composite nanoparticles, *Analyst*, 2011, 136, 1783-1798.

2 N. Kaji, Y. Okamoto, M. Tokeshi, Y. Baba, Nanopillar, nanoball, and nanofibers for highly efficient analysis of biomolecules, *Chem. Soc. Rev.*, 2010, 39, 948-956.

3 J. E. Gagner, S.Shrivastava, X. Qian, J. S. Dordick, R. W. Siegel, Amphiphile nanoarchitectonics: from basic physical chemistry to advanced applications, *Phys. Chem. Chem. Phys.*, 2013, 15, 10580-10611.

4 K.Taekyeong, J. Ki-Seok, H.Kwang, K.Hyung Min, P.Juhun, S.Yung Doug, H.Seunghun, Multilayered nano-prism vertex tips for tip-enhanced Raman spectroscopy and imaging, *Analyst*, 2013, 138, 5588-5593.

5 F. Meng, Z. Zhong, Polymersomes spanning from nano- to microscales: Advanced vehicles for controlled drug delivery and robust vesicles for virus and cell mimicking, *J. Phys. Chem. Lett.*, 2011, 2, 1533-1539.

6 W.Chunyana , S. Valiyaveettil, Correlation of biocapping agents with cytotoxic effects of silver nanoparticles on human tumor cells, *RSC Adv.*, 2013, 3, 14329-14338.

7 B. Luan, R. Zhou, Nanopore-based sensors for detecting toxicity of a carbon nanotube to proteins. *J. Phys. Chem. Lett.*, 2012, 3, 2337-2341.

8 Y. Hongbin, F. Haiyu, W. Xiaohan, Y. Shuhong, Hierarchical assembly of micro-/nano-building blocks: bio-inspired rigid structural functional materials, *Chem. Soc. Rev.*, 2011, 40, 3764-3785.

9 S. P.Anthony, S. M. Draper, Nano/microstructure fabrication of functional organic material: Polymorphic structure and tunable luminescence, *J. Phys. Chem. C*, 2010, 114, 11708−11716.

10 R. Sood, C. Iojoiu, E. Espuche, F. Gouanvé, G. Gebel, H. Mendil-Jakani, S. Lyonnard, J. Jestin, Proton conducting ionic liquid doped nafion membranes: Nano-structuration, transport properties and water sorption, *J. Phys. Chem. C*, 2012, 116, 24413-24423.

11R.H. Chou, S.C. Hsieh, Y.L. Yu, Huang M.H., Y.C.Huang, Y.H.Hsieh, Fisetin inhibits migration and invasion of human cervical cancer cells by down-regulating urokinase plasminogen activator expression through suppressing the p38 MAPK-dependent NF-κB signaling pathway, *PLoS One*, 2013, 8,e71983.

12 Urokinase plasminogen activator system as a potential target for cancer therapy. A.H.Mekkawy, D.L. Morris., M.H.Pourgholami, *Future Oncol.*, 2009, 5,1487-1499.

13 B. Mishra, B. B. Patel, S. Tiwari, Colloidal nanocarriers: A review on formulation technology, types and applications toward targeted drug delivery, *Nanomedicine*, 2010, 6, 9-24.

14 D. B.Khadka, D. T. Haynie, protein- and peptide-based electrospun nanofibers in medical biomaterials, *Nanomedicine*, 2012, 8, 1242-1262.

15 A. Rangnekar, A. M. Zhang, S. S. Li, K. M. Bompiani, M. N. Hansen, K. V. Gothelf, B. A. Sullenger, T. H. LaBean, Increased anticoagulant activity of thrombin-binding DNA aptamers by nanoscale organization on DNA nanostructures, *Nanomedicine*, 2012, 8, 673-681.

16 E. S. Kawasaki, T. A. Player, Nanotechnology, nanomedicine, and the development of new, effective therapies for cancer, *Nanomedicine*, 2005, 1, 101-109.

17 P. Sundaram, J. Wower, M. E. Byrne, A nanoscale drug delivery carrier using nucleic acid aptamers for extended release of therapeutic, *Nanomedicine*, 2012, 8, 1143-1151.

18 L. Li, G. Cui, M. Zhao, Y. Wang, H. Wang, W. Li, S. Peng, Assembly of β-cyclo-dextrin with 3S-tetrahydro-β-carboline-3-carboxylic acid and self-assembly of 6-(3S-carboline-3-carboxylaminoethylamino)-6-deoxy-β-cyclodextrin: Approaches to enhance antioxidation stability and anti-thrombotic potency, *J. Phy. Chem. B*, 2008, 112, 12139-12147.

19 X. Ren, G. Cui, M. Zhao, C. Wang, S. Peng, Coordination of thrombolytic Pro-Ala-Lys peptides with Cu (II): Leading to nano-scale self-assembly, increase of thrombolytic activity and additional vasodilation, *J. Phys. Chem. B*, 2008, 112, 8174-8180.

20 A. Abelein, L. Lang, C. Lendel, A. Gräslund, J. Danielsson, Transient small molecule interactions kinetically modulate amyloid β peptide self-assembly, *FEBS Lett.*, 2012, 586, 3991-3995.

21 A. Sood, M. Abid, S. Hailemichael, M. Foster, B. Török, M. Török, Effect of chirality of small molecule organofluorine inhibitors of amyloid self-assembly on inhibitor potency, *Bioorg. Med. Chem. Lett.*, 2009, 19, 6931-6934.

22 A. Kühnle, Self-assembly of organic molecules at metal surfaces, *Curr. Opin. Colloid Int.*, 2009, 14, 157-168.

23 J. B. Matson, R. H. Zha, S. I. Stupp, Peptide self-assembly for crafting functional biological materials, *Curr. Opin. Solid State Mater. Sci.*, 2011, 15, 225-235.

24 Y. Wang, J. Wu, G. Kang, M. Zhao, L. Gui, N. Li, L. Peng, X. Zhang, L. Li, S. Peng, Novel nano-materials, RGD-tetrapeptide-modified 17β-amino-11α-hydroxyandrost-1,4-diene-3-one: Synthesis, self-assembly based nano-images and in vivo anti-osteoporosis evaluation, *J. Mater.*

Chem., 2012, 22, 4652-4659.

25 M. Persson, A. Kjaer, Urokinase-type plasminogen activator receptor (uPAR) as a promising new imaging target: potential clinical applications, *Clin. Physiol. Funct. Imaging*, 2013, 33, 329-337.

26 C. Dellas, D.J. Loskutoff, Historical analysis of PAI-1 from its discovery to its potential role in cell motility and disease, *Thromb. Haemostasis*, 2005, 93, 631-640.

27 P.A. Andreasen, PAI-1-a potential therapeutic target in cancer, *Curr. Drug Targets*, 2007, 8, 1030-1041.

28 M.W. Gramling, F.C. Church, Plasminogen activator inhibitor-1 is an aggregate response factor with pleiotropic effects on cell signaling in vascular disease and the tumor microenvironment, *Thromb. Res.*, 2010, 125, 377-381.

29 K. Bajou, V. Masson, R.D. Gerard, P.M. Schmitt, V. Albert, M. Praus, L.R. Lund, T.L. Frandsen, N. Brunner, K. Dano, N.E. Fusenig, U. Weidle, G. Carmeliet, D. Loskutoff, D. Collen, P. Carmeliet, J.M. Foidart, A. Noël, The plasminogen activator inhibitor PAI-1 controls in vivo tumor vascularization by interaction with proteases, not vitronectin: implications for antiangiogenic strategies, *J. Cell Biol.*, 2001, 152, 777-784.

30 G.A. McMahon, E. Petitclerc, S. Stefansson, E. Smith, M.K. Wong, R.J. Westrick, D. Ginsburg, P.C. Brooks, D.A. Lawrence, Plasminogen activator inhibitor-1 regulates tumor growth and angiogenesis, *J Biol. Chem.*, 2001, 276, 33964-33968.

31 M.K. Durand, J.S. Bødker, A. Christensen, D.M. Dupont, M. Hansen, J.K. Jensen, S. Kjelgaard, L. Mathiasen, K.E. Pedersen, S. Skeldal, T. Wind, P.A. Andreasen, Plasminogen activator inhibitor-I and tumour growth, invasion, andmetastasis, *Thromb. Haemostasis*, 2004, 91, 438-449.

32 S. Lobov, M. Ranson, Molecular competition between plasminogen activator inhibitors type-1

and -2 for urokinase: Implications for cellular proteolysis and adhesion in cancer, *Cancer Lett.*, 2011, 303, 118-127.

33 Y. Jing, K. Kovacs, V. Kurisetty, Z. Jiang, N. Tsinoremas, J.R. Merchan, Role of plasminogen activator inhibitor-1 in urokinase's paradoxical in vivo tumor suppressing or promoting effects, *Mol. Cancer Res.*, 2012, 10, 1271-1281.

34 V. Pillay, C. R. Dass, P. F.M. Choong, The urokinase plasminogen activator receptor as a gene therapy target for cancer, *Trends Biotechnol.*, 2006, 25, 33-39.

35 C. E. de Bock, Y. Wang, Clinical significance of urokinase-type plasminogen activator receptor (uPAR) expression in cancer, *Med. Res. Rev.*, 2004, 24, 13-39.

36 A.P. Mazar, The urokinase plasminogen activator receptor (uPAR) as a target for the diagnosis and therapy of cancer, *Anti-Cancer Drug*, 2001, 12, 387-400.

37 H. Matthews, M. Ranson, J. D.A. Tyndall, M. J. Kelso, Synthesis and preliminary evaluation of amiloride analogs as inhibitors of the urokinase-type plasminogen activator (uPA), *Bioorg. Med. Chem. Letters*, 2011, 21, 6760-6766.

38 A. H. Shamroukh, M. El-Shahat, J. Drabowicz, M. M. Ali, A. E. Rashad, H. S. Ali, Anticancer evaluation of some newly synthesized N-nicotinonitrile derivative, *Eur. J. Med. Chem.*, 2013, 69, 521-526.

39 J. Liu, Y. Wang, Y. Yang, X. Jiang, M. Zhao, W. Wang, G. Wu, J. Wu, M. Zheng, S. Peng. Pyrolo[1,2:4,5]-1,4-dioxopyrazino[1,2:1,6]pyrido[3,4-b]indoles: A group of urokinase inhibitors, their synthesis and stereochemistry- dependent activity, *Chem. Med. Chem.*, 2011, 6, 2312-2322.

40 S. Mei, J. Liu, M. Zhao, W. Wang, Y. Wang, G. Wu, M. Zheng, S. Peng. From Cerius^2 based stereoview to mouse and enzyme: The model systems for discovery of novel urokinase inhibitors, *Mol. Biosyst.*, 2011, 7, 2664 - 2669.

41 X. Zhang, Y. Yang, M. Zhao, L. Liu, M. Zheng, Y. Wang, J. Wu, S. Peng, A class of Trp-Trp-AA-OBzl: Synthesis, *in vitro* anti-proliferation/*in vivo* anti-tumor evaluation, intercalation-mechanism investigation and 3D QSAR analysis, *Eur. J. Med. Chem.*, 2011, 46, 3410-3419.

42 H. Zhu, Y. Wang, Y. Wang, S.i Zhao, M. Zhao, L. Gui, W. Xu, X. Chen, Y. Wang, S. Peng, Folded conformation, cyclic pentamer, nano-structure and PAD4 binding mode of YW3-56, *J. Phys. Chem. C,* 2013, 117, 10070-10078.

43. S. Jin, Y. Wang, H. Zhu, Y. Wang, S. Zhao, M. Zhao, J. Liu, J. Wu, W. Gao, S. Peng, Nano-Sized Aspirin-Arg-Gly-Asp-Val: Delivery of aspirin to thrombus by a target carrier Arg-Gly-Asp-Val tetrapeptide, *ACS Nano*, 2013, 7, 7664 - 7673.